

NUMERICAL STUDY OF EFFECTS OF PULSATILE AMPLITUDE FOR TRANSITIONAL TURBULENT PULSATILE FLOW IN PIPES WITH RING-TYPE CONSTRICTIONS

T.S. LEE* AND Z.D. SHI

Mechanical and Production Engineering Department, National University of Singapore, Singapore 119260, Singapore

SUMMARY

The effects of pulsatile amplitude on sinusoidal transitional turbulent flows through a rigid pipe in the vicinity of a sharp-edged mechanical ring-type constriction have been studied numerically. Pulsatile flows were studied for transitional turbulent flow with Reynolds number (Re) of the order of 10^4 , Womersley number (N_w) of the order of 50 with a corresponding Strouhal number (St) of the order of 0.04. The pulsatile flow considered is a sinusoidal flow with dimensionless amplitudes varying from 0.0 to 1.0. Transitional laminar and turbulent flow characteristics in an alternative manner within the pulsatile flow fields were observed and studied numerically. The flow characteristics were studied through the pulsatile contours of streamlines, vorticity, shear stress and isobars. It was observed that fluid accelerations tend to suppress the development of flow disturbances. All the instantaneous maximum values of turbulent kinetic energy, turbulent viscosity, turbulent shear stress are smaller during the acceleration phase when compared with those during deceleration period. Various parametric equations within a pulsatile cycle have also been formulated through numerical experimentations with different pulsatile amplitudes. In the vicinity of constrictions, the empirical relationships were obtained for the instantaneous flow rate (Q), the pressure gradient (dp/dz), the pressure loss (P_{loss}), the maximum velocity (V_{max}), the maximum vorticity (ζ_{max}), the maximum wall vorticity ($\zeta_{w,max}$), the maximum shear stress (τ_{max}) and the maximum wall shear stress ($\tau_{w,max}$). Elliptic relation was observed between flow rate and pressure gradient. Quadratic relations were observed between flow rate and the pressure loss, the maximum values of shear stress, wall shear stress, turbulent kinematic energy and the turbulent viscosity. Linear relationships exist between the instantaneous flow rate and the maximum values of vorticity, wall vorticity and velocity. The time-average axial pressure gradient and the time average pressure loss across the constriction were observed to increase linearly with the pulsatile amplitude. Copyright © 1999 John Wiley & Sons, Ltd.

KEY WORDS: pulsatile flow; ring-type constriction; orifice; turbulent flow

1. INTRODUCTION

In recent years, pulsatile flows have attracted much attention due to their increasing relevance in many engineering and biomedical applications. For example, unsteady flow through constrictions is of interest to the designer of unsteady flow meters [1]. The relationship between flow rate and pressure loss across various type of mechanical constrictions provides a mean of

* Correspondence to: Mechanical and Production Engineering Department, National University of Singapore, Singapore 119260, Singapore.

estimating the mean flow rate from the measured pressure loss. The characteristics of unsteady/pulsatile turbulent flows observed can also be used for improvement of transportation of non-Newtonian fluid through miniature pulsatile pumps. The increase in flow rate of non-Newtonian materials of the same pressure gradient is possible with pulsating flow when compared with steady flow. Masry and Shobakys [2] reported that the energy saving can be as high as 30% if an optimum frequency of pulsatile velocity is used. An experimental study of pulsatile flow in pipes within the transition range was made by Einav and Sokolov [3]. The principle of unsteady flow was also frequently applied to the heat transfer devices, since heat transfer can be enhanced by the incipience of flow instability induced by undulating constrictions in the flow [4].

For biomedical applications with non-ring type constrictions in vascular pipes, research investigations are numerous [5–13]. Study on the characteristics of unsteady flow in the vicinity of ring type constrictions in vascular pipe are of interest to the designer of artificial heart valves and miniature pulsatile blood flow meters [1,14]. The possibility that hemodynamic factors may participate in the genesis and proliferation of atherosclerosis has also fostered increased study of flow through various types of constrictions during the past decade [15]. One of the recent research interest concerns the relationship between the vascular disease and the effects of constrictions and the magnitude of wall shear stress. It is, therefore, worthwhile from the fluid dynamics point of view to study and identify regions of very high shear and normal stresses in the flow (haemolysis), regions of very low or very high shear stress at walls (atheromatous lesions), and the extent of separated or reversed flow regions (thrombosis) in vascular pipes with implanted mechanical constrictions.

In the study of intracardiac blood flow and large vascular stenosis, the pressure loss, maximum flow velocity and shear stress and recirculation region are parameters of extreme interest because of their relation with the atheroma caused by large pressure drop across the constriction created through artificial implants, the corpuscle damage by large shear stress and the thrombus phenomena resulting from the recirculation region [12,16–23]. In some related studies, parameters of special interest are the pulsating frequency (St or Nw) and the pulsatile amplitude (A) [1,4,14,17,20].

Most of the existing studies were for laminar flows through constrictions with 'smooth' sinusoidal or bell shape profiles. Few considered transitional turbulent flow over mechanical constrictions with sharp edges. An investigation is thus carried out here to study the effect of pulsating flow on the developing flow characteristics of an unsteady transitional turbulent flow through a mechanical sharp edge ring type constriction (Figure 1(a)). As sinusoidal pulsatile inflow is the most common type of unsteady flow approximated in most engineering applications, it is also used here as an inflow boundary condition. The pulsatile flow in rigid pipe with a sharp edge ring-type constriction can also be used as a model for studying the application of fluid device implants in intracardiac flow, unsteady flow meters, as well as unsteady flow through heat exchangers.

With the sinusoidal inflow imposed as boundary condition for the pulsatile flow over a mechanical sharp edge ring-type constriction, the present investigation focused on the study of the variation of the pressure gradient along the axial direction, the pressure loss in flow passing through the constriction, the maximum flow velocity, maximum vorticity and maximum shear stress, the recirculation length, as well as the centreline velocity profiles in the developing flow. The results of the ring-type constriction presented here is for a constriction opening of $d/D = 0.5$ and thickness of $h/D = 0.1$. The mean turbulent flow Reynolds number is of the order 10^4 and the flow Strouhal number (St) considered is of the order 0.04 with a

corresponding Womersley number (N_w) of order 50. The pulsating amplitude (A) of the sinusoidal inflow considered varies from 0.0 to 1.0.

2. GOVERNING EQUATIONS AND NUMERICAL PROCEDURES

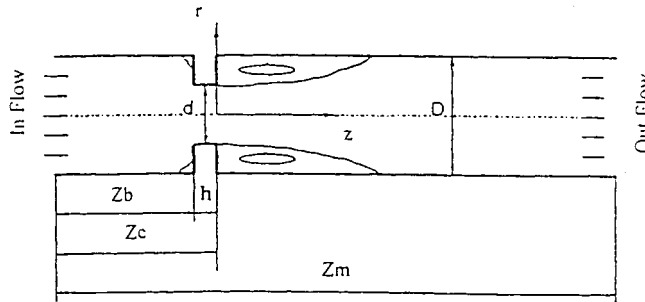
Incompressible turbulent flow in pipes near a mechanical sharp-edged constriction (Figure 1(a)) is governed by the Reynolds-averaged Navier–Stokes equations. By using the eddy viscosity concept and the $k-\epsilon$ turbulence model closure, the dimensionless governing equations of two-dimensional flow can be expressed in axisymmetric co-ordinates as follows:

Continuity equation:

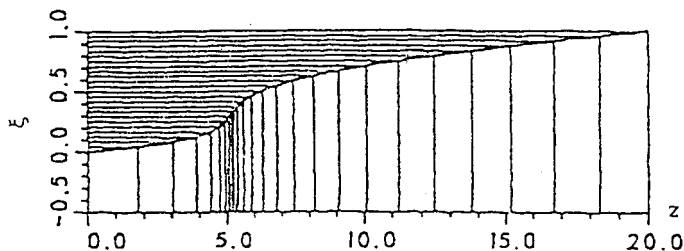
$$\frac{\partial}{\partial z} (ru) + \frac{\partial}{\partial r} (rv) = 0; \tag{1}$$

z -momentum equation:

$$St \frac{\partial u}{\partial t} + \frac{1}{r} \frac{\partial}{\partial z} (ru^2) + \frac{1}{r} \frac{\partial}{\partial r} (ruv) = -\frac{\partial p}{\partial z} + \frac{1}{r} \frac{\partial}{\partial z} \left(2rv_e \frac{\partial u}{\partial z} \right) + \frac{1}{r} \frac{\partial}{\partial r} \left[rv_e \left(\frac{\partial u}{\partial r} + \frac{\partial v}{\partial z} \right) \right]; \tag{2}$$



(a) Geometrical configuration



(b) Grid distribution along axial direction

Figure 1. Flow in rigid pipe with a sharp-edged ring-type constriction.

r -momentum equation:

$$St \frac{\partial v}{\partial t} + \frac{1}{r} \frac{\partial}{\partial z} (ruv) + \frac{1}{r} \frac{\partial}{\partial r} (rv^2) = -\frac{\partial p}{\partial r} + \frac{1}{r} \frac{\partial}{\partial z} \left[rv_e \left(\frac{\partial v}{\partial z} + \frac{\partial u}{\partial r} \right) \right] + \frac{1}{r} \frac{\partial}{\partial r} \left(2rv_e \frac{\partial u}{\partial r} \right) - v_e \frac{2v}{r^2}; \quad (3)$$

Turbulence kinetic energy equation:

$$St \frac{\partial k}{\partial t} + \frac{1}{r} \frac{\partial}{\partial z} (ruk) + \frac{1}{r} \frac{\partial}{\partial r} (rvk) = \frac{1}{r} \frac{\partial}{\partial z} \left(r \frac{v_t}{\sigma_k} \frac{\partial k}{\partial z} \right) + \frac{1}{r} \frac{\partial}{\partial r} \left(r \frac{v_t}{\sigma_k} \frac{\partial k}{\partial r} \right) + v_t G - \varepsilon; \quad (4)$$

Turbulence dissipation rate equation:

$$St \frac{\partial \varepsilon}{\partial t} + \frac{1}{r} \frac{\partial}{\partial z} (rue) + \frac{1}{r} \frac{\partial}{\partial r} (rve) = \frac{1}{r} \frac{\partial}{\partial z} \left(r \frac{v_t}{\sigma_\varepsilon} \frac{\partial \varepsilon}{\partial z} \right) + \frac{1}{r} \frac{\partial}{\partial r} \left(r \frac{v_t}{\sigma_\varepsilon} \frac{\partial \varepsilon}{\partial r} \right) + v_t C_1 \frac{\varepsilon}{k} G - C_2 f_c \frac{\varepsilon^2}{k}. \quad (5)$$

The effective viscosity v_e is defined as:

$$v_e = v_t + 1/Re, \quad (6)$$

where $1/Re$ represents the contribution of the fluid molecular viscosity, and v_t is the dimensionless turbulent eddy viscosity, defined by

$$v_t = C_\mu k^2 / \varepsilon. \quad (7)$$

The variable G in source terms of the k - ε equations is given as:

$$G = 2 \left[\left(\frac{\partial u}{\partial z} \right)^2 + \left(\frac{\partial v}{\partial r} \right)^2 + \frac{v^2}{r^2} \right] + \left(\frac{\partial u}{\partial r} + \frac{\partial v}{\partial z} \right)^2. \quad (8)$$

The values of the five empirical constants in the k - ε equations as given by Stevenson *et al.* [16] and Patankar [24] are:

$$C_\mu = 0.09, \quad C_1 = 1.44, \quad C_2 = 1.92, \quad \sigma_k = 1.0, \quad \sigma_\varepsilon = 1.3.$$

The parameter f_c in the ε -equation represents the streamline curvature correction for the standard k - ε model, and is defined in [25,26] as:

$$f_c = 1.0 - C_c R_{it}, \quad C_c = 0.2, \quad R_{it} = \frac{k^2 u^2 + v^2}{\varepsilon^2 R_c^2}, \quad (9)$$

where R_{it} is the turbulent Richardson number, R_c is the local streamline curvature, given by:

$$R_c = \left[uv \left(\frac{\partial v}{\partial r} - \frac{\partial u}{\partial z} \right) + u^2 \frac{\partial v}{\partial z} - v^2 \frac{\partial u}{\partial r} \right] / (u^2 + v^2)^{1.5}. \quad (10)$$

In the numerical process, these equations are reformulated in a curvilinear co-ordinate system with the axisymmetric physical components taken as the dependent variables. The transformed equations were expressed in a general semi-strong conservation form similar to that given by Lou and Yang [21] and Reggio *et al.* [27]. The resulting non-linear transformed equations are then solved by an iterative process. All the physical variables (u , v , p , k , ε) are updated as:

$$\phi^{n+1} = \phi^n + \delta\phi, \quad (11)$$

where n and $(n+1)$ are the last and current iteration numbers, and ϕ represents each of the physical variables. Substituting Equation (11) into the governing equations, the equations are then expressed in incremental form. The resulting equations are solved by the SIMPLE algorithm of Patankar [24] on *co-located* non-staggered grid for ease of imposing the pressure boundary conditions. All terms containing incremental variables are discretized by three-point

difference schemes. The first-order hybrid up-wind difference schemes are used for convective terms, the second-order central schemes for diffusive terms, the first-order forward schemes for pressure terms and first-order backward schemes for continuity equation. The residuals (R) are calculated by the second-order difference schemes, which are the second-order upwind scheme for convective terms, the central schemes for diffusive terms, and the second-order forward or backward schemes for pressure terms and continuity equations. Due to the variation of the main flow direction in pulsatile flows, the discretization of pressure gradient terms and continuity equations are adjusted according to the instantaneous main flow direction. A modified Crank–Nicolson scheme with a weighting factor θ is used to discretize the time-dependent terms in the governing equations. In the present work, $\theta = 0.6$ is adopted after a series of numerical tests. *The values of time step increment Δt chosen follows closely the general CFL criteria.* At convergence, the residual vector R approaches zero and the convergent results approach the second-order accuracy.

3. GEOMETRICAL CONFIGURATION AND BOUNDARY CONDITIONS

The geometrical parameters are defined in Figure 1(a). The constriction has opening ratio of 0.5 and thickness ratio of 0.1. The grid point in the r -direction is equally distributed. A stretching function described in detail in [14] and, as shown in Figure 1(b), is used for the grid points distribution in the z -direction. In the solution domain shown in Figure 1(a), the velocity profiles at the upstream inlet boundary are described by

$$u(r, t) = \frac{(n+1)(2n+1)}{2n^2} \bar{u}(t) \left(1 - 2 \frac{r}{D}\right)^{1/n}, \quad (12a)$$

where n is given a value of 6.0 in the present study. This power law, rather than a parabolic profile, is used at every time step because the velocity profiles of pulsatile flow are generally not parabolic. The average inlet velocity, $\bar{u}(t)$, is specified accordingly to the *sinusoidal pulsatile flow*:

$$\bar{u}(t) = 1 + A \sin(2\pi t/T). \quad (12b)$$

At each time step, along the solid wall, a no-slip velocity condition is used, i.e. $u = 0$, $v = 0$. Along the central line, axisymmetric conditions are applied for all variables, that $\partial u/\partial r = 0$, $v = 0$, $\partial p/\partial r = 0$, $\partial k/\partial r = 0$, $\partial \varepsilon/\partial r = 0$. At the downstream exit section, the pressure is fixed to zero. The flow is considered as fully developed, so all other variable's first-order differential along the z -direction are set to zero. The boundary conditions at the inlet section and k , ε wall boundary conditions are described as follows.

The k and ε at the inlet section are given by following formula as [28]:

$$k = C_\mu^{-1/2} l_m^2 \left(\frac{\partial u}{\partial r}\right)^2 \quad \text{and} \quad \varepsilon = C_\mu^{1/2} k \frac{\partial u}{\partial r}, \quad (13)$$

where the mixing length, l_m , is the smaller value determined by either the Nikuradse formula:

$$\frac{l_m}{D} = 0.07 - 0.04 \left(1 - \frac{2y}{D}\right)^2 - 0.03 \left(1 - \frac{2y}{D}\right)^4 \quad (14a)$$

or computed from the wall region formula:

$$l_m = 0.41y, \quad (14b)$$

where y is a normal distance from the wall. These formulations give zero values for k and ε at the center of the vascular pipe which is not realistic. To compensate for the possibility of unrealistic centerline values, a minimum value of the turbulent intensity of $0.003\bar{u}(t)$ was determined [28]. A long computing vascular pipe region upstream of the constriction is also used in the present calculation to minimise this effect.

Along the solid wall, a wall function is used to obtain the k and ε values at those grid points adjacent to the solid wall. Dou [29] proposed an analytical function to connect the u^* , u_p and y^+ for the whole flow region as follows:

$$\frac{u_p}{u^*} = 2.5 \ln(1 + y^+/5) + 7.05 \left(\frac{y^+/5}{1 + y^+/5} \right)^2 + 2.5 \left(\frac{y^+/5}{1 + y^+/5} \right) - B^*, \quad (15)$$

where B^* is the effect of wall roughness and is equal to zero in the present study. The u_p is the velocity component parallel to solid wall. The k and ε values at the corresponding grid points are then calculated as:

$$k = u^{*2}/\sqrt{C_\mu}, \quad \varepsilon = \lambda u^{*3}/(0.41y), \quad \nu_t = C_\mu k^2/\varepsilon, \quad (16)$$

where

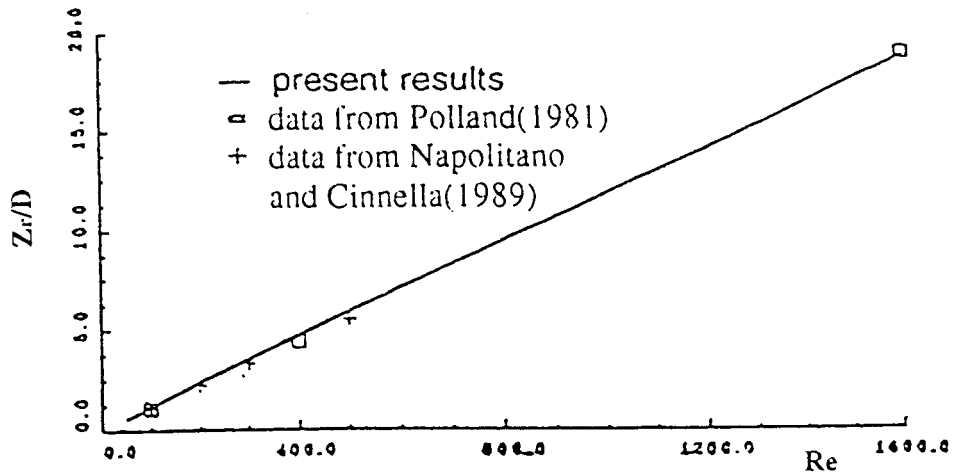
$$\lambda = \frac{2}{1 + 5/y^+} + 0.008(23.2 - y^+)(y^+)/(1 + y^+/5)^3.$$

4. RESULTS AND DISCUSSIONS

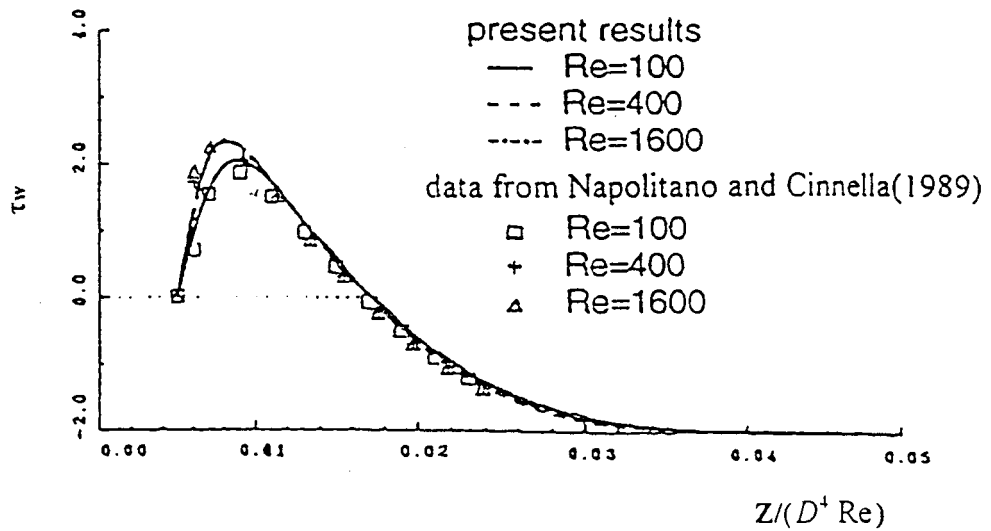
For the computation of flow field in the pipe with a ring-type constriction, non-uniform grids were used in the axial z -direction with more grid points being distributed nearer the constriction as shown in Figure 1(b). For the radial direction and the time domain, computational grids were evenly distributed. Grids with 21, 31, 41, 51 and 61 points in the r -direction and 101, 151, 201, 251 and 301 points in the z -direction were tested for 21, 31, 41, 51 and 61 time intervals per pulsatile period (T) in the time domain for the first three time periods to check on the grid point and time steps independency on the numerical results obtained. Further computations are then based on a grid point arrangement of 51, 201, 41 in the r -, z - and t -directions respectively. Computations were carried out for more than one periodical time cycle for every pulsatile unsteady flow conditions considered.

As there are no available unsteady flow cases similar to the problems considered here in the literature, the validity of the numerical procedure and grid size used were verified against available data for steady flow in a sudden expansion pipe. Test results are compared with data available from Polland [30] and Napolitano and Cinnella [31] for the recirculation length and the wall shear stress. These are shown in Figure 2. The results indicate that the present numerical procedure and grid size used produce accurate results when compared with known steady flow data. As each step of the unsteady flow cases considered here can be regarded as a quasi-steady state problem, it is thus assumed here that a similar procedure and grid size used should also produce accurate results for the unsteady flow cases to be considered here.

In this study, sinusoidal flow field with dimensionless amplitude A varying from 0.0 to 1.0 were computed. The effect of amplitude on the pulsatile turbulent flow field are numerically studied for pulsatile flow in a pipe with ring-type constriction. The mean flow Reynolds number is 10^4 and the Strouhal number is 0.04 with a corresponding Womersley number of



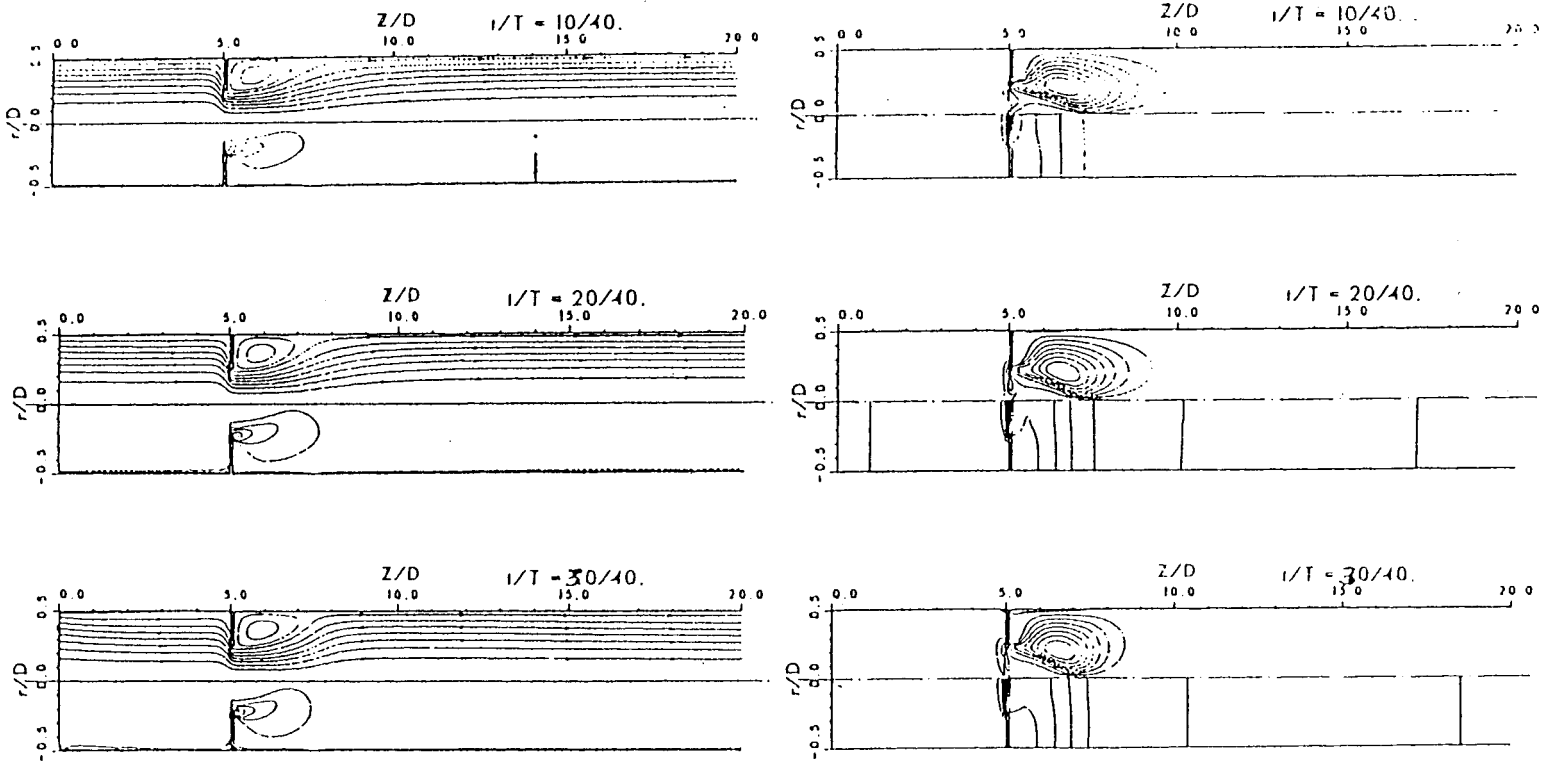
(a) Recirculation lengths



(b) Wall shear stress distribution

Figure 2. Comparison of results on steady flow in pipe with sudden expansion.

50. The instantaneous bulk velocity is expressed as $\bar{u}(t) = 1 + A \sin(2\pi t/T)$. The solution domain is r/D from 0.0 to 0.5, z/D from 0.0 to 20 with the constriction locating at $z/D = 5.0$ and t/T from 0.0 to 1.5. The constriction opening ratio is 0.5 and thickness ratio is 0. 1.



(a) Streamlines(upper half) and vorticity contours(lower half)

(b) Turbulent shear stress contours(upper half) and isobars(lower half)

Figure 3. Sinusoidal flow development in pipe with a ring-type constriction: $d/D = 0.5$, $h/D = 0.1$, $Re = 10^4$, $St = 0.04$, $A = 0.75$.

4.1. Turbulent pulsatile flow in tube with a ring-type constriction

4.1.1. Flow development. The general flow development of pulsatile flow is illustrated here for the case with $Re = 10^4$, $Nw = 50$ and $St = 0.0398$, with $A = 0.75$ for one pulsating cycle. The pulsatile flow developments are presented in Figure 3. The forward flow has its maximum instantaneous flow rate at $t/T = 1/4$, and minimum flow rate at $t/T = 3/4$. The recirculation length (z_r/D) varies within the range of 1.48–2.21. The shear stress contours contain a core-like feature consistently downstream of the constriction in the whole pulsating cycle, as shown in Figure 3(b). For $t/T > 4/4$, the second cycle starts and the flow repeats the similar structure. There is no constant recirculation region in the pulsatile flow. The reattached point moves forward and backward with time.

4.1.2. Centreline velocity and turbulent kinetic energy. The centreline velocity is also an important flow characteristics in the study of unsteady flow field development. Figure 4 presents the development of centreline velocity and turbulent kinematic energy with respect to time (t) for the case of $A = 1.0$. In general, it was observed that flow accelerates rapidly in a small upstream region of the constriction but decelerates gradually to a fully developed state downstream of the straight pipe flow. The centreline kinetic energy has two peaks. One is at the position of constriction and the other is near the axial position of recirculation point. Figure 4 shows that as t varies from 0 to 10, the flow accelerates to its maximum flow rate and the centreline velocity has its maximum value of 10.8 at $t = 10$. As the flow undergoes a

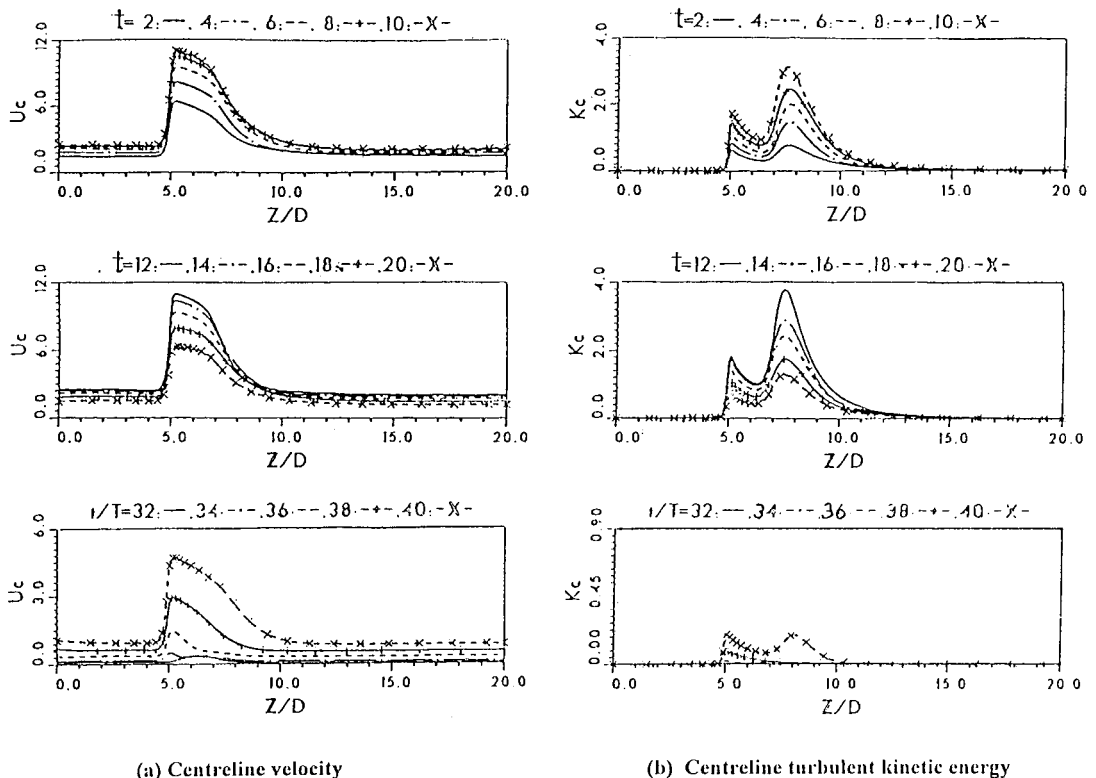


Figure 4. Development of centreline velocity and turbulent kinetic energy: $d/D = 0.5$, $h/D = 0.1$, $Re = 10^4$, $St = 0.04$, $Nw = 50.1$, $A = 1.0$.

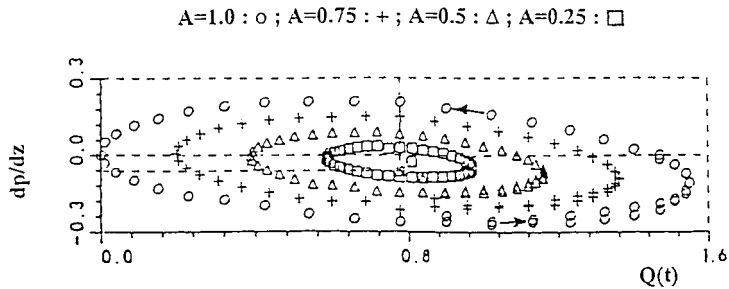


Figure 5. Relation between flow rate and axial pressure gradient. (Arrows show increment with respect to time)

deceleration period from $t=20$ to 30 , both the velocity and kinetic energy decrease. The minimum velocity and kinetic energy appear at $t=32$. With the bulk velocity approaching zero, the recirculation length also approaches zero. When t increases from 30 to 50 , flow accelerates to its peak flow rate again. For $t=50-60$, flow undergoes another acceleration and deceleration cycle.

4.2. Parametric relations of turbulent pulsatile flows in pipe with a ring-type constriction

4.2.1. Relation between flow rate (Q) and pressure gradient (dp/dz). The relation between flow rate (Q) and pressure gradient (dp/dz) along the axial direction in the fully developed region is presented in Figure 5. The peak dp/dz value appears at the instant of zero flow rate (Q), when the flow has its maximum acceleration or deceleration. Conversely, $dp/dz=0$ occurs at the instant of maximum flow rate, when the flow acceleration is equal to zero. Hence, characteristics of the pressure gradient (dp/dz) depends mainly on the flow acceleration or deceleration. The dp/dz has the same absolute values for the same acceleration and deceleration. For the sinusoidal flow, this relation can be expressed as:

$$\left(\frac{dp/dz}{C_{pz1}}\right)^2 + \left(\frac{Q}{C_{pz2}}\right)^2 = 1, \quad (17)$$

where C_{pz1} , and C_{pz2} are constants depending on the magnitude of A .

Typical relations between the instantaneous flow rate (Q) and axial pressure gradient (dp/dz) in a fully developed flow region at $z/D=16$ is shown on Figure 5. The phase angle, ϕ_{p-Q} , between flow rate and axial pressure gradient is about 85° . All the instantaneous points form nearly elliptic curves.

The time-average pressure gradient ($\overline{dp/dz}$) is calculated by:

$$\overline{dp/dz} = \frac{1}{T} \int_{0.5T}^{1.5T} (dp/dz) dt \quad (18)$$

and the results are presented in Figure 6. With the increase of amplitude, $\overline{dp/dz}$ decreases. The dimensional time-average pressure gradient is calculated by:

$$\overline{dp/dz}^* = \overline{dp/dz} (Re\mu)^2 / (\rho D^3). \quad (19)$$

Hence, with an increase of pulsating amplitude, more energy is required in the transportation of fluid in straight pipe.

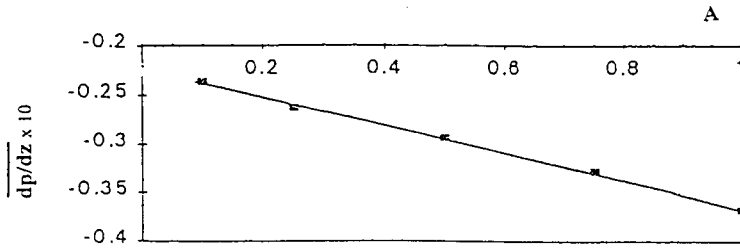


Figure 6. Effect of pulsating amplitude on time averaged axial pressure gradient.

A=1.0 : o ; A=0.75 : + ; A=0.5 : Δ ; A=0.25 : □

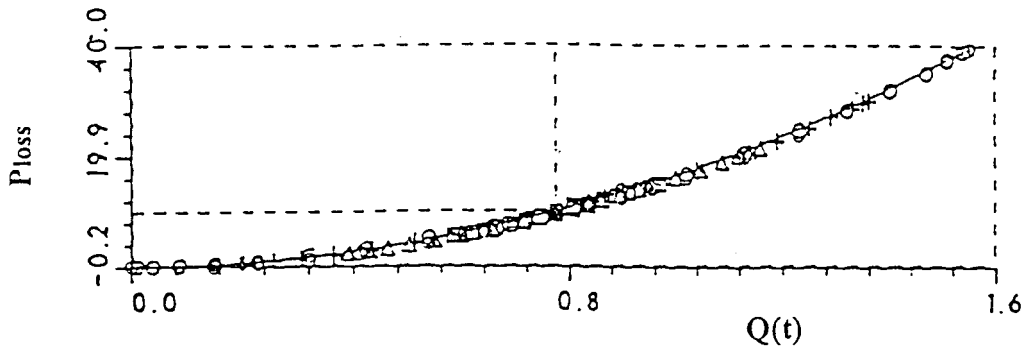


Figure 7. Relation between flow rate and pressure loss across constriction.

4.2.2. *Relations between flow rate and pressure loss.* The results of pressure loss are presented in Figure 7 for flows at different amplitude values. These data form a fitting curves of:

$$P_{\text{loss}} = 16.4Q|Q|. \tag{20}$$

Variations of time-average pressure loss (\bar{P}_{loss}) with respect to pulsatile amplitude is shown in Figure 8. The \bar{P}_{loss} increases with the pulsatile amplitude. Through other studies, it is

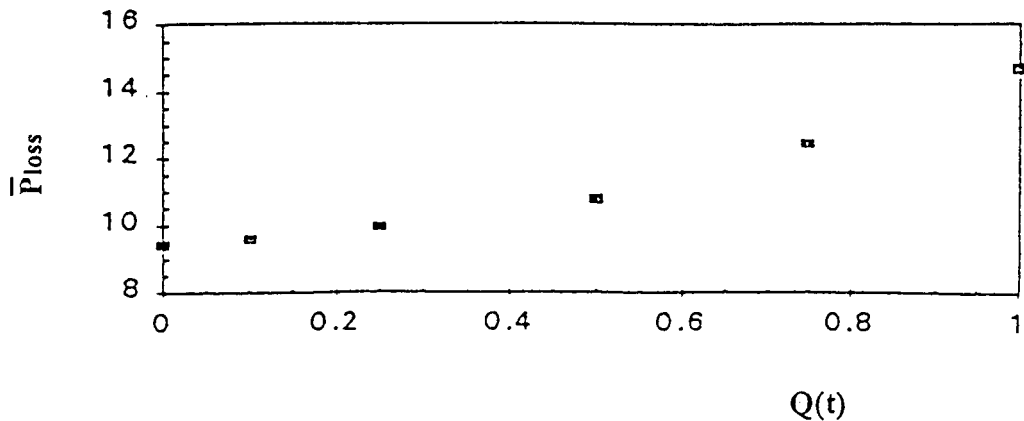


Figure 8. Effect of pulsating amplitude on time average pressure loss.

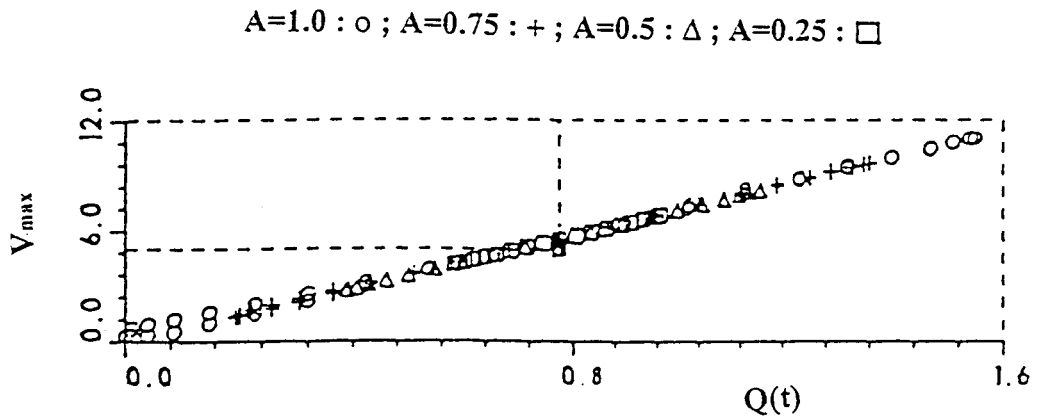


Figure 9. Relation between flow rate and maximum velocity.

generally noted that the difference between characteristics of (\bar{P}_{loss}) with respect to pulsatile amplitude are negligible for Strouhal number of 0.04 and another Strouhal number one order greater.

4.2.3. *Other parameters of the turbulent pulsatile flow.* Simple relations are found between flow rate and non-dimensional maximum values of flow velocity, vorticity, shear stress, turbulent kinetic energy and wall vorticity, wall shear stress as approximated related by:

$$\begin{aligned} u_{\text{max}} &= 7.50Q(t); & \Omega_{\text{max}} &= 283.7Q(t); & \tau_{\text{max}} &= -0.733Q^2(t); & k_{\text{max}} &= 1.98Q^2(t); \\ \Omega_{\text{w,max}} &= 44.7Q(t); & \tau_{\text{w,max}} &= -0.0257Q^2(t). \end{aligned} \quad (21)$$

The above relationships are also presented in Figures 9–14.

In physiological flow, turbulent shear stress is directly related to the cause of damage of blood cell. The numerical results of the instantaneous maximum values of the turbulent shear stress (τ_{max}) of the whole flow field, and the wall shear stress ($\tau_{\text{w,max}}$) are presented in Figures 12 and 13 respectively. The relation between Q and τ_{max} are complex. For the same Q value, the τ_{max} value is smaller during the acceleration than that during deceleration. This is similar to the phenomena discussed in the turbulent viscosity development. The wall shear stress $\tau_{\text{w,max}}$

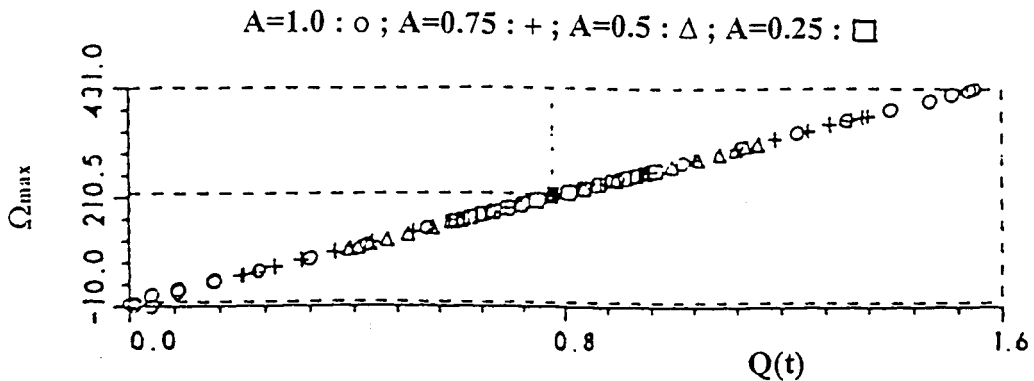


Figure 10. Relation between flow rate and maximum vorticity.

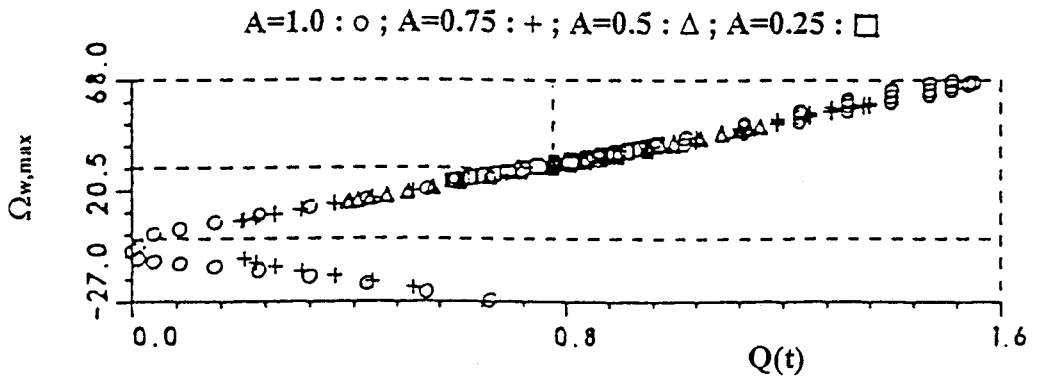


Figure 11. Relation between flow rate and maximum wall vorticity.

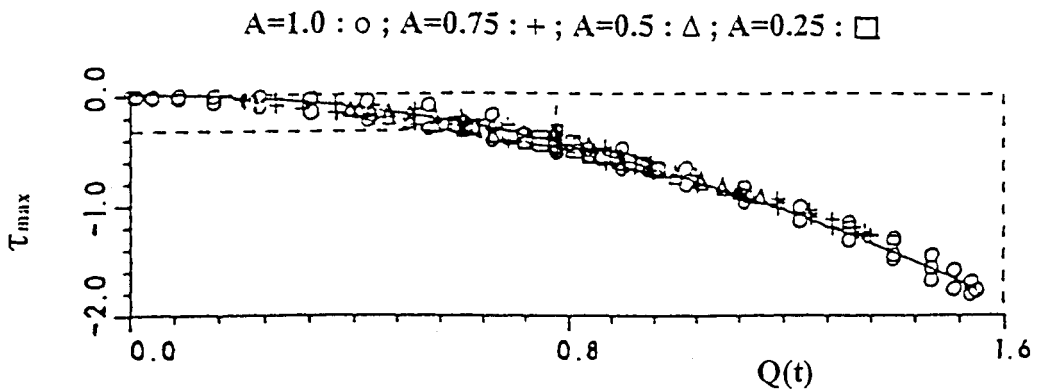


Figure 12. Relation between flow rate and maximum shear stress.

has a simple quadratic relationship with the flow rate. As shown in Figures 12 and 13, the maximum wall vorticity and shear stress are about 1/6 and 1/3 of their overall values respectively.

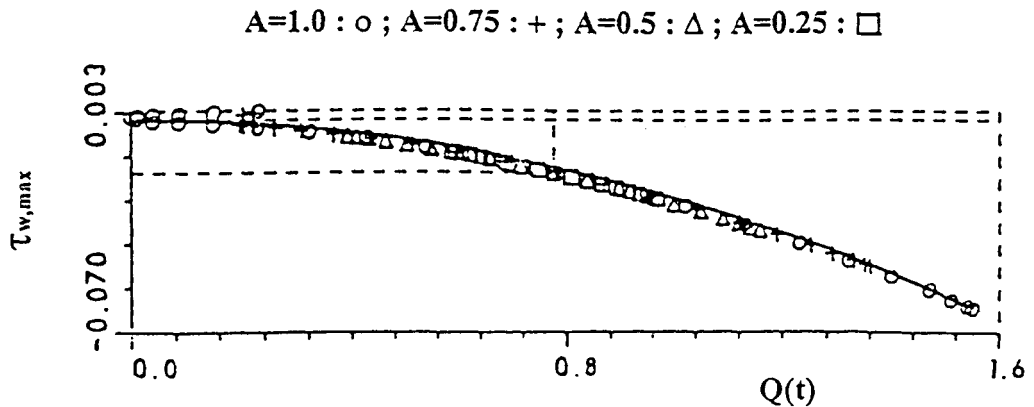


Figure 13. Relation between flow rate and maximum wall shear stress.

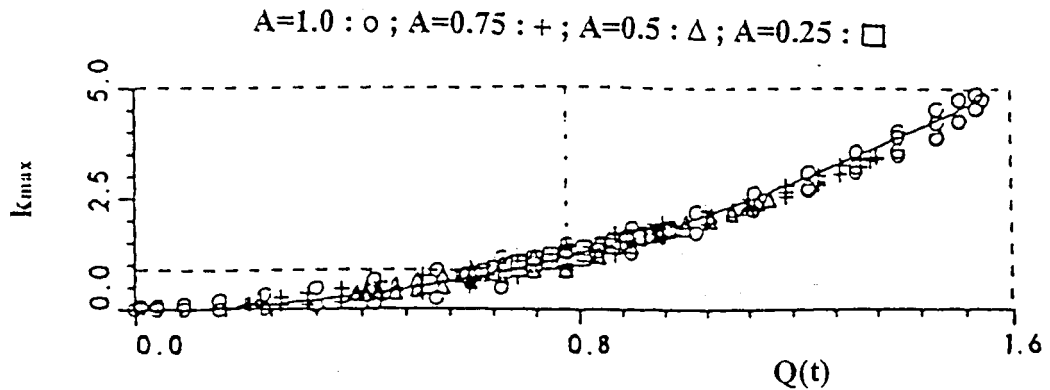


Figure 14. Relation between flow rate and maximum turbulent kinetic energy.

At $A = 1.0$, there is a short time period where the maximum turbulent kinetic energy is equal to zero, as shown in Figure 14. The flow field at this time period is then laminar.

Development of the characteristics of turbulence in the pulsatile flow field with time can be deduced from the relationship of the flow rate (Q) and the maximum turbulent viscosity ($v_{t,max}$) as shown in Figure 15. For the sinusoidal flow, the $v_{t,max}$ is consistently larger than zero, except during the initial starting phase of the pulsatile flow period. The flow in general has smaller $v_{t,max}$ value during the acceleration period when compared with the $v_{t,max}$ value during the deceleration period. The flow is in general turbulent for sinusoidal flow, with a minimum instantaneous $v_{t,max}$ value of the order 0.010.

4.3. Application of present results to biomedical and intracardiac flow phenomena

For cases corresponding to intracardiac flow and valvular regurgitation, the blood can be considered as Newtonian fluid in the larger artery, where the shear rate is larger [16,18,32]. At 36–37°C, the blood density (ρ) is $1.055 \times 10^3 \text{ kg m}^{-3}$ and the kinematic viscosity, ν , is 0.04 Poise or $3.79 \times 10^{-6} \text{ m}^2 \text{ s}^{-1}$. The peak velocity at mitral valve opening section is about $3.0\text{--}6.0 \text{ m s}^{-1}$. The artery diameter is about $2.0 \times 10^{-2}\text{--}3.0 \times 10^{-2} \text{ m}$ and the corresponding peak Reynolds number (Re) are in the order of 10^4 . The normal physiological frequency is about 72 beats min^{-1} or 1.2 Hz, which gives the corresponding Womersley number ($D\sqrt{\omega/\nu}$)

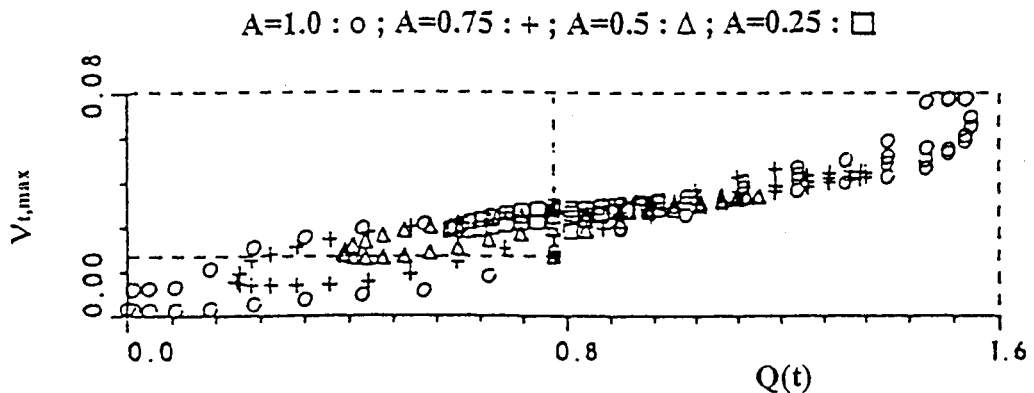


Figure 15. Relation between flow rate and maximum turbulent viscosity.

of the order of 50.0. The above range of parameters were considered in the present study. Only the general trends of the results are presented in this paper.

Development of non-invasive quantification method is of interest in valvular regurgitant diagnosis applications [33]. Based on the free turbulent jet flow theory, Slordahl *et al.* [34] developed a method to evaluate the regurgitant quantity as:

$$Q = C_d A_o [2\Delta p / \rho]^2, \quad (22)$$

where Q is the regurgitant volume, C_d is the 'discharge coefficient', A_o is the valve opening area, ρ is the density of blood, Δp is the pressure difference across the valve, and C_d is equal to 0.61. However, the difficulty in obtaining Δp on human patients [35] prevents its practical applications.

Cape [36] developed a non-invasive method to evaluate the regurgitant volume as:

$$Q = \int u^2 dA / U_o = \pi U_m^2 X^2 / (26.46 U_o), \quad (23)$$

where U_m is the central-line velocity at axial location X , U_o is the maximum velocity at the valve. This result is applicable in clinical diagnosis because the velocity information can be obtained by using Doppler echocardiography technique.

Issaz [37] also developed a theoretical model for the non-invasive assessment of the transmitral pressure–flow relation. According to the linear momentum equation applied to the atrioventricular coupling, the left-atrium – left-ventricle pressure difference ($p_a - p_v$) can be written as:

$$p_a - p_v = A \partial v / \partial t + Bv^2 + Cv, \quad (24)$$

where v is the transmitral blood velocity and A , B and C are variables related to the geometry of the atrium, ventricle and mitral orifice respectively, which can be obtained from Doppler echocardiography.

In the present study, with the opening ratio of 0.5, the relationships between the flow rate and the maximum of velocity, turbulent shear stress, pressure loss can be obtained. These relationships are given by

$$Q = 0.1333 V_{\max}; \quad P_{\text{loss}} = 16.4Q|Q|; \quad \tau_{w,\max} = -0.0257Q|Q|. \quad (25)$$

Hence, from the velocity information of Doppler echocardiography, the regurgitant volume, pressure difference, the maximum shear stress and wall shear stress can be predicted.

In the valvular regurgitant and intracardiac flow, the turbulent shear stress and pressure loss across constrictions are of relevant to the endothelium, the damage of corpuscles and the development of atheroma respectively. By using the numerical results of the pulsatile flows, the shear stress and the pressure loss can be estimated. The dimensional maximum shear stress reaches 596 N m^{-2} for both $Nw = 30$ and 50 . The dimensional maximum wall shear stress is 24.0 N m^{-2} for both $Nw = 30$ and 50 . The time period of shear stress greater than 40 N m^{-2} , where endothelium will be deteriorated, is about $0.5T$. The dimensional maximum pressure loss across constriction is $1.27 \times 10^4 \text{ N m}^{-1}$ or 95.3 mmHg for both $Nw = 30$ and 50 . This value is greater than 30 mmHg , where the atheroma appears.

Consider the two parameters of pressure loss and turbulent shear stress for the case of $Re = 10^4$ and $D = 2.50 \times 10^{-2} \text{ m}$. The dimensional pressure loss is given by:

$$P_{\text{loss}} = 16.4Q|Q|. \quad (26)$$

The value of the peak pressure loss is $2.674 \times 10^4 \text{ N m}^{-1}$ or 200.7 mmHg . This value is large enough to cause the atheroma, which is developed at pressure drop greater than 30 mmHg . At $Q = 0.5Q_{\max}$, the pressure drop is equal to 50.2 mmHg , which is also larger than the critical value.

The dimensional wall shear stress is given by

$$\tau_{w,\max} = -0.0257Q|Q|. \quad (27)$$

The peak wall shear stress value is equal to 47.81 N m^{-2} , which is near to the critical value of endothelium deterioration, of 40 N m^{-2} . The peak dimensional turbulent shear stress is equal to $1.115 \times 10^3 \text{ N m}^{-2}$. This value is much larger than the critical value of the incipient hemolysis at 400 N m^{-2} . At $Q = 0.5Q_{\max}$, the turbulent shear stress is equal to 418.1 N m^{-2} and also greater than the critical value.

5. CONCLUSIONS

Pulsatile turbulent flows in pipe with a ring-type constriction have been computed for a Reynolds number (Re) of the order of 10^4 and a Womersley number (Nw) of 50 with a corresponding Strouhal number (St) of 0.04. The pulsating flows are sinusoidal in nature with different amplitude (A). In general, numerical experimentations show that flow deceleration in the pulsatile cycles tends to enlarge the recirculation region and its effect becomes more significant with the increase of the pulsatile amplitudes (or the corresponding increase in Womersley and Strouhal numbers). The corresponding flow acceleration in the pulsatile cycles tends to increase the pressure drop in the pipe flow. The time-averaged pressure gradient along the axial direction decreases linearly while the pressure loss increases parabolically when the pulsatile amplitude was increased from 0.0 to 1.0.

For the pulsatile flow considered here, the flow in the vicinity of the pipe with ring-type constrictions is observed to be always turbulent after the pulsatile flow was initiated. The flow disturbance is not diminished completely because the time period with small velocity in each the cycle is very short. For the symmetrical sinusoidal pulsatile flows investigated, they exhibit both laminar and turbulent flow characteristics in an alternative manner within the pulsatile flow fields. The length of the laminar core in the pulsatile flow, as shown through the turbulent shear stress contours, were observed to change in magnitude and domain with respect to time in a systematic manner.

Various parametric flow relationships are obtained to describe the pulsatile flow characteristics. Numerical linear relationships are obtained for the flow rate and the maximum values of velocity, vorticity. Quadratic relationships are obtained for the flow rate and the pressure loss across the constriction, and the maximum wall shear stress. An elliptic relationship is observed between flow rate and pressure gradient. From the flow characteristics obtained, flow acceleration was observed to suppress the development of flow disturbance in the pulsatile flows studied here. All the instantaneous maximum values of turbulent kinetic energy, turbulent viscosity, turbulent shear stress are smaller during the acceleration phase when compared with those during deceleration period.

ACKNOWLEDGMENTS

The authors gratefully acknowledge the financial assistance of the National University of Singapore through a research grant [RP3972715]. The assistant of Dr SH Winoto and Mr T.W. Ng are also gratefully acknowledged.

APPENDIX A. NOMENCLATURE

a	pulsatile amplitude
A	pulsatile amplitude, $A = a/D$

C_c, C_μ, C_1, C_2	coefficients of turbulence model
D	vascular pipe diameter, used as the characteristic length, L
d	orifice diameter
dp/dz	pressure gradient in axial direction
$\overline{dp/dz}$	time-averaged pressure gradient, $1/T \int_t^{t+T} (dp/dz) dt$
f_μ	coefficient of turbulence model
h	constriction thickness
h_o	obstacle height, $h_o = (D-d)/2$
k	dimensionless turbulence kinetic energy
Nw	Womersley number, $Nw = D\sqrt{\omega/\nu}$
p	dimensionless pressure
P_{loss}	pressure loss across constriction
	pressure difference between upstream and downstream flow
$\overline{P}_{\text{loss}}$	time-averaged pressure loss, $1/T \int_t^{t+T} P_{\text{loss}} dt$
Q	flow rate, $Q = Q(t) = (\pi/4)D_u^2 \bar{u}(t)$
Q_{max}	dimensionless maximum flow rate = 1.0
Re	Reynolds number, $Re = \bar{u}_{\text{peak}} D/\nu$
R_{it}	Richardson number of streamline curvature
r	radial co-ordinate, radial distance
St	Strouhal number, $St = D/(\bar{u}_{\text{peak}} T) = (1/2\pi)(Nw^2/Re)$
T	time period of pulsatile flow cycle
T_s	time period of sinusoidal flow cycle
t	time co-ordinate
u	dimensionless axial velocity component
$\bar{u}(t)$	instantaneous bulk velocity in pipe
\bar{u}_{peak}	the peak $\bar{u}(t)$ value (used as characteristics velocity)
v	radial velocity component
z	axial co-ordinate, axial distance
z_r	recirculation length

Greek letters

α_d	under relaxation factor in updating the pressure
ε	dimensionless dissipation rate of turbulent energy
φ_{p-Q}	dimensionless vorticity, $\Omega = \partial u/\partial r - \partial v/\partial z$
ν	fluid molecular kinetic viscosity
ν_e	effective viscosity, $\nu_e = 1/Re + \nu_t$
ν_t	turbulent eddy viscosity
ρ	fluid density
τ	dimensionless shear stress, $\tau = \nu_e(\partial u/\partial r + \partial v/\partial z)$
ξ, η	co-ordinate variables in general curvature co-ordinate
Ω	phase angle between flow rate and pressure gradient variation in pulsatile flow

REFERENCES

1. E.H. Jones Jr. and R.A. Bajura, 'A numerical analysis of pulsating laminar flow through a pipe orifice', *J. Fluids Eng.*, **113**, 199–205 (1991).
2. O.A.El. Masry and K.El. Shobakys, 'Pulsating slurry flow in pipelines', *Exp. Fluids*, **7**, 481–486 (1989).

3. S. Einav and M. Sokolov, 'An experimental study of pulsatile pipe flow in the transition range', *ASME J. Biomech. Eng.*, **115**, 404–411 (1993).
4. H. Suzuki, Y. Inoue, T. Nishimura, K. Fukutani and K. Suzuki, 'Unsteady flow in a channel obstructed by a square rod (criss-cross motion of vortex)', *Int. J. Heat Fluid Flow*, **14**, 2–9 (1993).
5. J.S. Lee and Y.F. Fung, 'Flow in locally constricted tubes at low Reynolds numbers', *ASME J. Appl. Mech.*, **37**, 9–16 (1970).
6. J.S. Lee and Y.F. Fung, 'Flow in non-uniform small blood vessels', *J. Microvasc. Res.*, **3**, 272–287 (1971).
7. W.L. Oberkampf and S.C. Goh, 'Numerical solution of incompressible viscous flow in irregular tubes', *Proc. Int. Conf. on Computational Methods for Non-linear Mechanics*, University of Texas, Austin, 1974, pp. 569–579.
8. J.C. Bentz and N.A. Evans, 'Hemodynamic flow in the region of a simulated stenosis', American Society of Mechanical Engineers, Winter Annual Meeting, Houston, November 30–December 4, *ASME Paper No. 75-WA/BA10-10*, 1975.
9. M.D. Deshpande, D.P. Giddens and R.F. Mabon, 'Steady laminar flow through modelled vascular stenoses', *J. Biomech.*, **9**, 165–174 (1976).
10. V. O'Brien and L.W. Ehrlich, 'Simple pulsatile flow in an artery with a constriction', *J. Biomech.*, **18**, 117–127 (1985).
11. S.C. Dreumel and G.D.C. Kuiken, 'Steady flow through a double converging–diverging tube model for mild coronary stenoses', *J. Biomech. Eng.*, **111**, 212–221 (1989).
12. T.S. Lee, 'Numerical studies of fluid flow through tubes with double constrictions', *Int. J. Numer. Methods Fluids*, **11**, 1113–1126 (1990).
13. T.S. Lee and H.T. Low, 'Separation and reattachment of fluid flow through series vascular constriction', *J. Finite Elem. Anal. Des.*, **18**, 365–377 (1994).
14. T.S. Lee, 'Numerical study of effects of pulsatile amplitude on unsteady laminar flows in rigid pipe with ring-type constrictions', *Int. J. Numer. Methods Fluids*, **24**, 275–290 (1997).
15. L.H. Back, J.R. Radbill and Y.I., 'Measurement and prediction of flow through a replica segment of a mildly atherosclerotic coronary artery of man', *J. Biomech.*, **19**, 1–17 (1986).
16. D.M. Stevenson, A.P. Yoganathan and F.P. Williams, 'Numerical simulation of steady turbulent flow through triflate aortic heart valves-II. Results on five models', *J. Biomech.*, **18**, 909–926 (1985).
17. L.M. Srivastava, 'Flow of couple stress fluid through stenotic blood vessels', *J. Biomech.*, **18**, 479–485 (1985).
18. H. Huang, V.J. Modi, B.R. Seymour and R. Raliga, 'Fluid dynamics of stenosed arteries: a numerical study', *The Proceedings of 6th International Conference on Biomedical Engineering*, 1990, pp. 535–540.
19. H.W. Sung and A.P. Yoganathan, 'Secondary flow velocity patterns in a pulmonary artery model with varying degrees of valvular pulmonic stenosis: pulsatile *in vitro* studies', *ASME J. Biomech. Eng.*, **112**, 88–92 (1990).
20. N. Masahide and S. Tadashi, 'Numerical study on the unsteady flow of non-Newtonian fluid', *ASME J. Biomech. Eng.*, **112**, 100–103 (1990).
21. Zheng Lou and Wen-Jei Yang, 'A computer simulation of the non-Newtonian blood flow at the aortic bifurcation', *J. Biomech.*, **26**, 37–49 (1993).
22. D.A. Steinman, Bach Vinh, C.R. Ethier, M. Ojha, R.S.C. Cobbold and K.W. Johnston, 'A numerical simulation of flow in a two-dimensional end-to-side anastomosis model', *ASME J. Biomed. Eng.*, **115**, 112–118 (1993).
23. T.S. Lee, 'Steady laminar fluid flow through variable constrictions in vascular tubes', *J. Fluids Eng.*, *ASME*, **116**, 66–71 (1994).
24. S.V. Patankar, *Numerical Heat Transfer and Fluid Flow*, Hemisphere, Washington, DC, 1980.
25. T. Tangsanchali and S. Maheswaran, '2D depth-averaged flow computation near groyne', *J. Hydraul. Eng.*, **116**, 71–81 (1990).
26. S.K. Dong and M.K. Chung, 'Curvature corrections to Reynolds stress model for computation of turbulent recirculation flows', *AIAA J.*, **30**, 2968–2969 (1992).
27. M. Reggio, M. Agouzoul and R. Camarero, 'Computation of incompressible turbulent flows by an opposed-differencing scheme', *Numer. Heat Transf.*, **12**, 307–320 (1987).
28. R.S. Amano and H. Brandt, 'Numerical study of turbulent axisymmetric jets impinging on a flat plate and flowing into an axisymmetric cavity', *ASME J. Fluid Eng.*, **106**, 410–417 (1984).
29. G.R. Dou, 'The turbulence structure of opening channel and pipe flows', *Sci. China*, **11**, 1115–1124 (1980) (in Chinese).
30. A. Pollard, 'A contribution on the effects of inlet conditions when modelling stenosis using sudden expansions', *J. Biomech.*, **14**, 349–355 (1981).
31. M. Napolitano and P. Cinnella, 'A numerical study of planar and axially-symmetric sudden expansion flows', *Comput. Fluids*, **17**, 185–193 (1989).
32. B. Diebold, A. Delouche, P.H. Dumeé, J.P. Guglielmi, P.H. Delouche and P. Peronneau, '*In-vitro* analysis of a model of intracardiac jet: analysis of the central core of axisymmetric jets', *J. Biomech.*, **23**, 35–44 (1990).
33. A.S. Pearlman and C.M. Otto, 'Quantification of valvular regurgitation: a review of cardiovascular ultrasound', *Echocardiography*, **4**, 271–287 (1987).
34. A. Slordahl, J.E. Solbakken, H. Piene, B.A.J. Angelsen, O. Rossroll and S.O. Samstad, 'Quantification of aortic regurgitation by Doppler echocardiography: a new method evaluated in pigs', *Med. Biol. Eng. Comput.*, **28**, 300–305 (1990).
35. S.O. Wille, 'Pressure and flow in arterial stenoses simulated in mathematical models', *Appl. Math. Model.*, **4**, 483–488 (1980).
36. E.G. Cape, 'A new theoretical model for non-invasive quantification of mitral regurgitation', *J. Biomech.*, **23**, 27–33 (1990).
37. K. Isaaz, 'A theoretical model for the non-invasive assessment of the transmitral pressure–flow relations', *J. Biomech.*, **25**, 581–590 (1992).